catalysts

MDPI

Review

Hierarchical Ternary Sulfides as Effective Photocatalyst for Hydrogen Generation Through Water Splitting: A Review on the Performance of $ZnIn_2S_4$

Ravichandran Janani [1], Raja Preethi V [1], Shubra Singh [1,*], Aishwarya Rani [2] and Chang-Tang Chang [2,*]

[1] Crystal Growth Centre, Anna University, Chennai, Tamil Nadu 600025, India; jananikrishnaveni@gmail.com (R.J.); preethivenkat888@gmail.com (R.P.V.)
[2] Department of Environmental Engineering, National I-Lan University, Yilan 260, Taiwan; r0824013@niu.edu.tw
* Correspondence: shubra6@gmail.com or shubra6@annauniv.edu (S.S.); ctchang@niu.edu.tw (C.-T.C.); Tel.: +91-0-44-22358316 (S.S.); +886-639357400 (C.-T.C.)

Abstract: One of the major aspects and advantages of solar energy conversion is the photocatalytic hydrogen generation using semiconductor materials for an eco-friendly technology. Designing a low-cost efficient material to overcome limited light absorption as well as rapid recombination of photogenerated charge carriers is essential to achieve considerable hydrogen generation. In recent years, sulfide based semiconductors have attracted scientific research interest due to their excellent solar response and narrow band gap. The present review focuses on the recent approaches in the development of hierarchical ternary sulfide based photocatalysts with a special focus on $ZnIn_2S_4$. We also observe how the electronic structure of $ZnIn_2S_4$ is beneficial for water splitting and the various strategies involved for improving the material efficiency for photocatalytic hydrogen generation. The review places emphasis on the latest advancement/new insights on $ZnIn_2S_4$ being used as an efficient material for hydrogen generation through photocatalytic water splitting. Recent progress on essential aspects which govern light absorption, charge separation and transport are also discussed in detail.

Keywords: water splitting; hydrogen; photocatalyst; visible light response; ternary chalcogenides; heterostructure; doping effect

Citation: Janani, R.; Preethi V, R.; Singh, S.; Rani, A.; Chang, C.-T. Hierarchical Ternary Sulfides as Effective Photocatalyst for Hydrogen Generation Through Water Splitting: A Review on the Performance of $ZnIn_2S_4$. *Catalysts* **2021**, *11*, 277. https://doi.org/10.3390/catal11020277

Academic Editors: Bruno Fabre and Edward Gillan

Received: 31 December 2020
Accepted: 15 February 2021
Published: 19 February 2021

1. Introduction

Depletion of fossil fuels and deterioration of energy supply demands a better solution for sustainable energy, driving extensive research on the use of Hydrogen (H_2) as an alternate energy source. The conversion of sunlight and water, two major resources of energy on earth, into H_2 has been advocated as an ideal goal in providing a clean and green energy system without compromising environmental safety. The utilization of solar energy to dissociate water into H_2 and oxygen (O_2) through photocatalysis assisted by a semiconductor photocatalyst is gaining momentum among various ways of H_2 production. With the pioneering work from Honda and Fujishima on the splitting of water using single-crystal TiO_2 [1,2], many revolutionary ideas have contributed towards developing an efficient photocatalyst for the effective utilization of solar energy and high H_2 yield in absence of any carbonaceous by-products [3–6]. The mechanism of photo splitting of water involves absorption of radiation with an energy greater than the band-gap of the photocatalyst. It mainly consists of two half-reactions: oxidation of water to form O_2 and the reduction of protons to form H_2 [7–15]

$$H_2O + h^+_{vb} \rightarrow 2H^+ + \frac{1}{2} O_2 \text{ [Photooxidation of water]} \quad (1)$$

$$2\,H^+ + 2\,e^-_{cb} \rightarrow H_2 \text{ [Photoreduction of protons]} \quad (2)$$

These redox reactions can be initiated only when the positions of the conduction band (CB) is more negative than H_2 evolution potential (0V vs Normal Hydrogen Electrode (NHE)) and the valence band (VB) is more positive than the water oxidation potential (+1.23 V Vs NHE) [16]. For photo-assisted water splitting, oxide semiconductors continue to hold a reputation due to their ease of availability, low cost and photostability. Various oxide semiconductors, especially oxides consisting of metal cations (Ga^{3+}, In^{3+}, Ge^{4+}, Sn^{4+}, Sb^{5+}) with d^{10} configuration and metal cations (Ti^{4+}, Zr^{4+}, Nb^{5+}, Ta^{5+}, W^{6+}) with d^0 configuration have been reported for good photocatalytic activity when assisted by co-catalyst like RuO_2 [17–23]. Perovskite structured metal oxides like $SrTiO_3$ and $KTaO_3$ can split water without an external bias in powdered form and show enhanced results when combined with NiO or Rh cocatalyst [24,25]. However, since their valence band comprises of deep 2p oxygen orbital, their O2p levels lie at a potential of 3 eV making the effective band-gap (E_g) to fall in the UV region (4% of the available spectra). For the efficient utilization of the solar spectrum, the band-gap of a photocatalyst should be in the visible region having E_g < 3 eV. This cultivates the need of material with a narrow band-gap having suitable valence band positions. In this regard, metal sulfides are known for their shallow valence band which consists of S3p levels at more negative potential when compared to O2p levels in metal oxides thereby narrowing the bandgap energy [26]. The suitable band edge positions in CdS with narrow band-gap energy ~2.4 eV makes it one of the most studied materials for solar water splitting application. Regardless of the benefits, CdS experiences photocorrosion that greatly eradicates its practical application. Sulfide ions present on the surface of CdS get easily oxidized by photogenerated holes to form solid sulfur which is irreversible [27]. Nevertheless, the development of a photocatalytic corrosion-resistant, visible light-absorbing material with enhanced photoactivity is the doorway to effectuate the cycle of converting sunlight to hydrogen. Hence in view of the prospective applications, ternary semiconductor chalcogenides with hierarchical structures are emerging with greater scope in photocatalysis [28]. Numerous investigations have claimed that the ternary metal sulfides ($ZnIn_2S_4$, $CdIn_2S_4$, $CaIn_2S_4$, $MgIn_2S_4$, etc) with AB_2X_4 (where A = Zn, Cd, Mg, Ca, B = Ga, In and C = S) structure could be a new class of potential visible-light active photocatalysts due to their appreciable chemical stability and optical band gaps. These ternary sulphide compounds with AB_2X_4 structure have been explored for photo-assisted decomposition of water as listed in Tables 1 and 2. Among the ternary metal sulfides, $ZnIn_2S_4$ is the only member of the family with a layered structure with potential applications in charge storage, opto-electronics and photoconduction [29]. In the hexagonal layered structure of $ZnIn_2S_4$, the atoms are arranged in layers along the c-axis. Zn atoms are tetrahedrally bonded to the S atoms (Zn-S_4) while the In atoms have two different environments, a tetrahedral arrangement with four S atoms (In-S_4) and an octahedral arrangement with 6 S atoms (In-S_6). This layered arrangement of atoms is responsible for the improved photocatalytic performance of $ZnIn_2S_4$ [30–32]. It has also been shown that the $ZnIn_2S_4$ structure initially shows a resistivity drop during the exposure to light creating electron/hole pairs. The doubly negative charged surface traps the holes leading to an enhanced free-electron transport to the surface [33]. It is also known that a photocatalyst with a p-block metal ion having d^{10} configuration exhibits good photocatalytic performance during water decomposition [18]. Hence, the presence of In^{3+} metal ions with d^{10} configuration in $ZnIn_2S_4$ could be promising for good photocatalytic activity for water decomposition. This review with detailed information on photocatalytic activity of various ternary semiconductor sulfide chalcogenides with hierarchical structures will give a bird's eye view on their performance with a special emphasis on $ZnIn_2S_4$.

Table 1. Photocatalytic activity of $ZnIn_2S_4$-based material in H_2 generation with respective parameters.

No.	Photocatalyst	Synthesis Method	Morphology	Co-Catalyst Used	Light Source	Sacrificial Agent	Catalyst Mass Used (g)	Yield (μmol h^{-1})	Ref.
1.	$ZnIn_2S_4$	CPBr assisted Hydrothermal	Flower like microspheres	-	250 W Hg lamp	Na_2SO_3/Na_2S	0.1	1544.8 (μmol g^{-1} h^{-1})	[34]
2.	$ZnIn_2S_4/MoSe_2$	Electrostatic self-assembly	Uniform sheet like structure	-	300 W Xe lamp	Lactic acid	0.005	6454	[35]
3.	$ZnIn_2S_4/g\text{-}C_3N_4$	Hydrothermal	Hierarchical sheets		300 W Xe lamp	Triethanolamine	0.005	14.1	[36]
4.	$g\text{-}C_3N_4/ZnIn_2S_4$	Hydrothermal	Micron-sized bulk morphology with sheets	-	300 W Xe lamp	Triethanolamine	0.05	2780	[37]
5.	2 wt% Y-$ZnIn_2S_4$	Hydrothermal	Microflowers with irregular opening	-	350 W Xe lamp	Na_2SO_3/Na_2S	0.2	155.9	[38]
6.	2 wt% Gd-$ZnIn_2S_4$	Hydrothermal	Rose like micro-clusters	-	350 W Xe lamp	Na_2SO_3/Na_2S	0.2	163.1	[38]
7.	2 wt% Er-$ZnIn_2S_4$	Hydrothermal	Microflowers and sheets of smaller width	-	350 W Xe lamp	Na_2SO_3/Na_2S	0.2	173.1	[38]
8.	2 wt% Ce-$ZnIn_2S_4$	Hydrothermal	Microflowers and sheets of smaller width	-	350 W Xe lamp	Na_2SO_3/Na_2S	0.2	181.7	[38]
9.	2 wt% La-$ZnIn_2S_4$	Hydrothermal	Completely developed microflower	-	350 W Xe lamp	Na_2SO_3/Na_2S	0.2	219.5	[38]
10.	1wt%La-$ZnIn_2S_4$	Hydrothermal	Self-organised microflowers	-	350 W Xe lamp	Na_2SO_3/Na_2S	0.2	583.4 (μmol g^{-1} h^{-1})	[39]
11.	$ZnIn_2S_4$-MoS_2	Microwave synthesis	Flower-like microflowers	-	150 W Xe lamp	Na_2SO_3/Na_2S	0.1	111.6 (μmol g^{-1} h^{-1})	[40]
12.	$Cd_xIn_2S_4$-$Zn_{1-x}In_2S_4$	Hydrothermal	Particle	-	500 W Xe lamp	Na_2SO_3/Na_2S	0.2	590 (μmol g^{-1} h^{-1})	[41]
13.	$ZnIn_2S_4$-MoS_2	Wet Chemical method	Flake like structure	-	300 W Xe lamp	Triethanolamine	0.025	8898 (μmol g^{-1} h^{-1})	[42]
14.	1wt%La1%rGO-$ZnIn_2S_4$	Hydrothermal	Hollow spheres loaded with sheets	-	350 W Xe lam	Na_2SO_3/Na_2S	0.2	2255 (μmol g^{-1} h^{-1})	[43]
15.	MoS_2/graphene/$ZnIn_2S_4$	Hydrothermal	Flower like microstructure	-	300 W Xe lamp	Na_2SO_3/Na_2S	0.05	4169	[44]

Table 1. *Cont.*

No.	Photocatalyst	Synthesis Method	Morphology	Co-Catalyst Used	Light Source	Sacrificial Agent	Catalyst Mass Used (g)	Yield (μmol h^{-1})	Ref.
16.	$ZnIn_2S_4$	Hydrothermal	-	Pt	300 W Xe lamp	Na_2SO_3/Na_2S	0.3	257 (μmol g^{-1} h^{-1})	[45]
17.	$ZnIn_2S_4$	Hydrothermal	Flower, nanoplates nanostrips	-	300 W Xe lamp	KOH (photodecomposition of H_2S)	0.5	5287 (μmol g^{-1} h^{-1})	[32]
18.	$ZnIn_2S_4$	Hydrothermal	Floriated microspheres	Pt	300 W Xe lamp	Na_2SO_3/Na_2S	0.1	8420 (μmol g^{-1} h^{-1})	[46]
19	$ZnIn_2S_4$	CTAB assisted Hydrothermal	Microspheres with petals	Pt	300 W Xe lamp	Na_2SO_3/Na_2S	0.2	62.25 (μmol g^{-1} h^{-1})	[47]
20.	$ZnIn_2S_4$	Surfactant assisted Hydrothermal	Microspheres with petals	Pt	300 W Xe lamp	Na_2SO_3/Na_2S	0.2	692 (μmol g^{-1} h^{-1})	[48]
21.	$ZnIn_2S_4$	microwave assisted Hydrothermal	Microclusters	Pt	300 W Xe lamp	Na_2SO_3/Na_2S	0.1	69.2	[49]
22.	$ZnIn_2S_4$	Solvothermal	Flowering cherry sphere like structure	Pt	300 W Xe lamp	Na_2SO_3/Na_2S	0.2	136.5 (μmol g^{-1} h^{-1})	[50]
23.	$ZnIn_2S_4$	Thermal Sulfidation	Irregular lumps in micro scalar size	Pt	300 W Xe lamp	Na_2SO_3/Na_2S	0.2	~55 (μmol g^{-1} h^{-1})	[51]
24.	$ZnIn_2S_4$/MWCNT	Hydrothermal	Floriated microspheres	-	300 W Xe lamp	Na_2SO_3/Na_2S	0.1	6840 (μmol g^{-1} h^{-1})	[52]
25.	$ZnIn_2S_4$/Fluoropolymer	Solvothermal/ polymerisation	Particles and flowers	-	350 W Xe lamp	Na_2SO_3/Na_2S	1.02	~398 (μmol g^{-1} h^{-1})	[53]
26.	$ZnIn_2S_4$/Transition metal loaded	CTAB assisted hydrothermal	Microspheres	Pt	300 W Solar simulator	Na_2SO_3/Na_2S	0.05	4000 (μmol g^{-1} h^{-1})	[54]
27.	Cu-$ZnIn_2S_4$	Hydrothermal	Microsphere with petals/sheets	Pt	300 W Xe lamp	Na_2SO_3/Na_2S	0.2	757.5 (μmol g^{-1} h^{-1})	[55]
28.	Ni-$ZnIn_2S_4$	Hydrothermal	Microsphere with petals/sheets	Pt	350 W Xe lamp	Na_2SO_3/Na_2S	0.2	~45 (μmol g^{-1} h^{-1})	[56]
29.	ZnS-$ZnIn_2S_4$	Solvothermal	Microspheres	Pt	400 W metal halide lamp	Glucose	0.1	103 (μmol g^{-1} h^{-1})	[28]

2. Crystalline Structures of Sulfide Based Photocatalysts

When a metal or semi-metal cation is combined with a sulfur anion, it forms a metal sulfide compound with a stoichiometry of M_xS_y (MS, M_2S, M_3S_4, MS_2). Bi-metal sulfides are formed in a similar approach with a stoichiometry of $A_{1-x}B_xS_y$, where x and y are integers [57]. The occupation of metal and sulfur atoms in metal sulfide are arrangements of a close-packed system with four notable structures (Figure 1a). In the first case, we have a symmetrical sodium chloride (NaCl) structure type with each ion occupying an octahedron position with six nearest neighbors. It is called the pyrite structure when the crystal comprises two sulfide ions in each octahedron position [57–59]. Then we have the sphalerite structure where the metal ions are bounded by six oppositely charged ions positioned tetrahedrally [60]. The next important structure type is called the fluorite, in which every metal cation is surrounded by eight anions and every anion, in turn, is surrounded by four cations. If this symmetry is reversed with every metal cation surrounded by four anions and every anion, in turn, is surrounded by eight cations, then it is called the anti-fluorite structure [57,61].

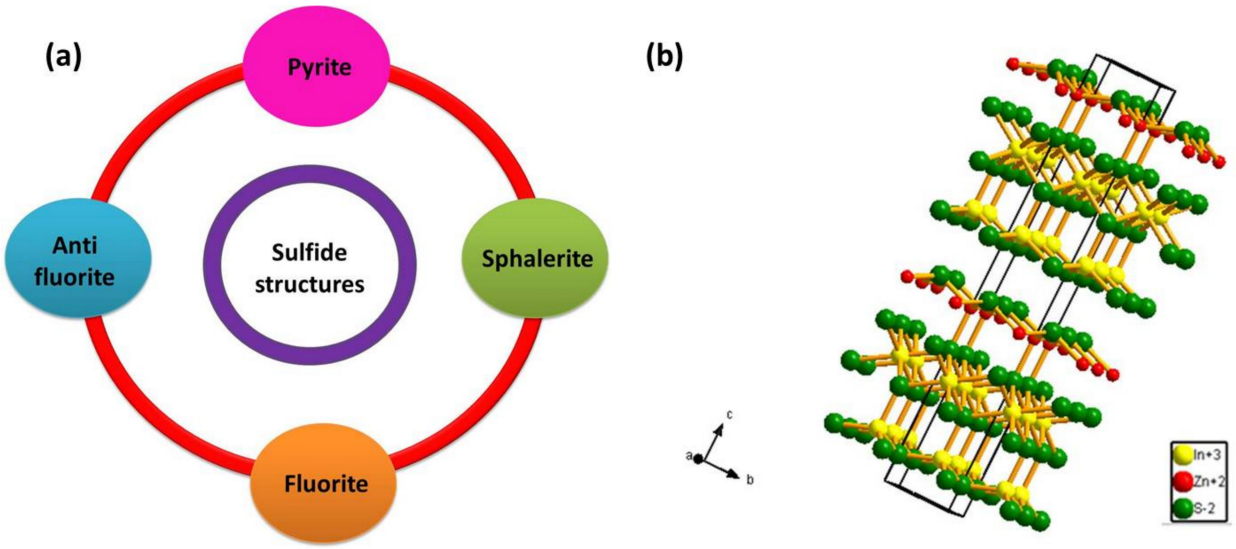

Figure 1. (**a**) Classification of sulfide compounds based on their structure. (**b**) The layered hexagonal structure of $ZnIn_2S_4$.

Another metal sulfide category has a cubic spinel structure possessing a stoichiometry of AB_2S_4, where A site is occupied by divalent metal ion (such as Mg, Zn, Fe, Cu etc) arranged tetragonally, while B site is occupied by trivalent metal ions (such as In, Cr, Ti, Co) arranged octahedrally [57]. The oxidation state adopted by sulfur is usually 2^- and hence to maintain the valence symmetry in the AB_2S_4 structure, the divalent A-site is occupied by cation with 2+ oxidation state and trivalent B-site is occupied by cation with 3+ oxidation state with the structure possibility of $A^{2+}B^{3+}S_4^{2-}$ [57]. These structures are called ternary metal chalcogenides. From among the family of AB_2S_4 semiconductors, $ZnIn_2S_4$ is the only member with a layered structure (see Figure 1b) [62]. It is a potentially visible-light-responsive photocatalyst reported with three different polymorphs, including, cubic, hexagonal and rhombohedral phase [63]. $ZnIn_2S_4$ displays less toxicity when compared to metal sulfides such as CdS and Sb_2S_3 while exhibiting similar optical properties which portrays the advantage of utilizing $ZnIn_2S_4$ in environmental remediation applications. Additionally, $ZnIn_2S_4$ can also be beneficial over ZnS with its narrow bandgap value reported between 2.06 eV–2.85 eV [63]. The splendid physical and chemical properties of $ZnIn_2S_4$ have attracted immense attention in various applications including H_2 generation [37–49], CO_2 reduction [64–66], environmental remediation [40] under visible light irradiation. The layer structured semiconductor $ZnIn_2S_4$ exhibiting cubic polymorph contains ABC stacking of S atoms with tetrahedral and octahedral coordination of Zn and

In atoms respectively, while the hexagonal phase consists of ABABA stacking of S atoms with Zn; half of the In atoms are coordinated tetragonally and the other half In atoms are coordinated octahedrally. The rhombohedral phase exhibits a strong Zn-S and In-S bond in the layer with a weaker S–S bond, with every S atom corresponding to a different layer [66]. The band structure of $ZnIn_2S_4$ has also been explored theoretically on the basis of Density Functional Theory (DFT) [55,64,67,68]. Studies suggest that $ZnIn_2S_4$ is a direct bandgap semiconductor as both VB and CB of $ZnIn_2S_4$ lie on G point of thee Brillouin zone [55]. Valence band consists mainly of S3p and Zn3d orbitals and the conduction band consists of hybridized In5s5p and S3p orbitals. Under photo illumination, electrons would transfer from the valence band to the conduction band leaving behind the photogenerated holes which are beneficial for photo-assisted water splitting [55].

3. Electronic Structure Beneficial for Water Splitting

Photocatalytic water splitting is an energetically uphill reaction (Gibbs energy = 237 kJ/mol) which involves positive energy change and multiple electron transfer similar to naturally occurring photosynthesis. Hence, photocatalytic water splitting is often referred to as "artificial photosynthesis" [69]. Theoretically, a material possessing a minimum bandgap of 1.23 eV is suitable for photochemical water splitting, as explained in Figure 2 [16].

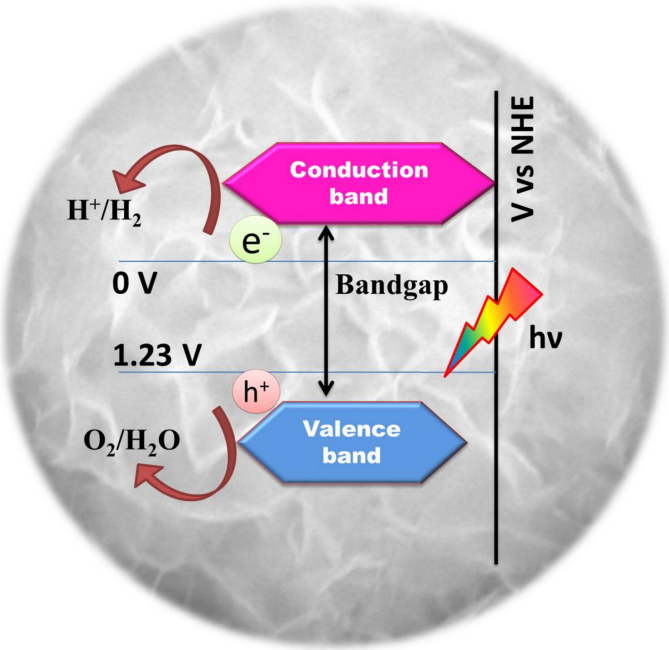

Figure 2. Schematic illustration of the essential electronic structure of a photocatalyst for water splitting.

Despite the fact that metal oxide photocatalysts are easily available, metal sulfides have attracted a lot of attention for their high absorbance in the 'hole controlled photocatalysis'. Notably, the photocatalytic activity depends on the quantity of photon absorption. In this regard, high absorbance materials like sulfides show better photocatalytic activity [69,70]. Ionic character in the range of 20–30% is essential for the increased photocatalytic activity of a catalytic material [70]. High ionic character is much needed for water adsorption on the catalyst surface in spite of the fact that the ionic character is responsive to surface corrosion. The majority of the oxide materials provide 50% ionic character attributed to their high electronegativity difference while sulfides also perfectly match this basic requirement [70]. A drawback with the oxide materials is that they face hydrogen embrittlement (metal hydride formation inside the lattice) due to the high affinity of hydrogen with oxygen. This leads to the reduction in catalyst durability in photocatalytic water splitting reactions.

Conversely, the rate of hydrogen embrittlement on the sulfide surface is comparatively lesser than the oxide surface [70].

4. Photocatalytic Hydrogen Evolution by $ZnIn_2S_4$

$ZnIn_2S_4$, a ternary compound of the AB_2X_4 family has been identified as a visible light photocatalyst with desirable band energy positions to split water photocatalytically. To achieve the same, various experimental synthesis techniques have been explored. Bai et al., [34] synthesized a series of flower-like $ZnIn_2S_4$ through surfactant-assisted hydrothermal method where the pH level of reactant played a major role in providing a maximum yield of H_2 about 1545 μmol g^{-1} h^{-1}. Photostable $ZnIn_2S_4$ [45] could produce H_2 through water reduction for at least up to 150 h. Chaudari et al., [32] have reported excellent photocatalytic activity of $ZnIn_2S_4$ for the production of H_2 through the splitting of H_2S. The quantity of the surfactant (triethylamine), solvent and the synthesis temperature both have a huge impact on the morphology of the product as well as the rate of H_2 production [45,50]. $ZnIn_2S_4$ synthesized at 160 °C at pH 1 showed 34.3% of apparent quantum yield. Among a series of surfactants used, a sample synthesized with cetyltrimethylammonium bromide (CTAB) is noted to have a larger d(006) space value [47]. It is claimed that larger d(006) space could promote higher separation of photogenerated charge carriers thereby enhancing the photocatalytic performance. Synthesis of $ZnIn_2S_4$ through thermal sulfidation at different temperatures provides clear insights into the phase change of the material from cubic to rhombohedral with respect to changes in the synthesis temperature [51]. This study provides a precise understanding of the effect of phase change on optical and photocatalytic properties of $ZnIn_2S_4$.

5. Strategies for Enhancing Photocatalytic Performance

In a typical photo-assisted water splitting process, a photocatalyst is excited with energy greater than or equal to the band-gap value to generate electron–hole pairs. These photogenerated charge carriers would migrate to the surface of the photocatalyst and react with the organic pollutant. Photogenerated electrons would reduce H^+ to H_2 whilst the holes would be consumed by the sacrificial agent added to the system. Though its bandgap lies in the visible region, $ZnIn_2S_4$ suffers from recombination of charge carriers as well as poor migration [63]. In order to improve the photocatalytic performance of $ZnIn_2S_4$, several approaches have been made including the formation of heterostructure with a suitable photocatalyst, doping with metal ions, surface modification, control of morphology etc. These modifications aid in improving the surface and optical properties of $ZnIn_2S_4$ and escalating migration of charge carriers with lower recombination rate resulting in enhanced photocatalytic activity.

5.1. Heterostructure Formation

A heterostructured photocatalyst is advantageous in the sense that it assists in extending the light absorption range and accelerates charge transfer. Building a heterojunction between $ZnIn_2S_4$ and other suitable semiconductors could facilitate band alignment which could suppress the recombination rate leading to enhanced photocatalytic performance. Lin et al., (2018) designed a heterojunction between g-C_3N_4/$ZnIn_2S_4$ achieving in-situ growth of $ZnIn_2S_4$ nano leaves on the surface of g-C_3N_4 nanosheets (Figure 3) via a one-step surfactant-assisted solvothermal method [37].

Pudkon et al., (2020) investigated the effect of coupling MoS_2 with $ZnIn_2S_4$ in H_2 generation. An improved H_2 generation of 200 μmol g^{-1} h^{-1} was observed with 40% loading of MoS_2 into $ZnIn_2S_4$ lattice due to the enhanced charge separation efficiency and transportation, as well as by charge recombination suppression at the contact interface between $ZnIn_2S_4$ and MoS_2 [40] Yuan et al., (2016) constructed MoS_2-graphene/$ZnIn_2S_4$ microarchitectures for the improved H_2 generation of 4167 μmol g^{-1} h^{-1}. The results reveal that the superior activity of the heterostructure is due to the positive synergetic effect between MoS_2 and graphene, where MoS_2 and graphene act as H_2 evolution reaction catalyst

and electron transfer bridge respectively [44]. Chai et al., (2012) fabricated a series of composite heterostructures between multiwall carbon nanotubes (MWCNT) and $ZnIn_2S_4$ via a facile hydrothermal method. It is envisaged that MWCNT electron-accepting and electron-transporting properties increase the life of electron-hole pairs generated by semiconductor thus helping in enhancing the photocatalytic property [52]. Experimental results suggest that 3% MWCNT embedded in the interior of $ZnIn_2S_4$ microspheres shows a maximum H_2 production rate of 684 μmol h^{-1} [52]. Fan et al., (2010) hydrothermally synthesized $ZnIn_2S_4$ and deposited it over electrospun poly(HFBA-co-MAA)/PVDF fibers [53]. Here Poly(HFBA-co-MAA) is referred to as Hexafluorobutylacrylate-co-methacrylic acid and PVDF is referred to polyvinylidene fluoride. It is suggested that the use of polymer-carriers has the advantages of being easy recycle, flexibility, excellent weatherability and large surface area. The growth of $ZnIn_2S_4$ microspheres on polymer surface (organic carrier) aids in photocorrosion resistance and enhances photocatalytic performance. $ZnIn_2S_4$/fluoropolymer fiber composites were able to produce 9.1 mL/h even when recycled up to three runs. On the other hand, Li et al., (2010) synthesized series of ZnS coated $ZnIn_2S_4$ via facile solvothermal synthesis using methanol as the solvent [28]. Among the samples synthesized with different mol% of ZnS loading, the sample with 17% ZnS loading showed better photocatalytic activity. In their investigation, glucose is used as a hole scavenger and acts as an electron donor to inhibit photocorrosion on the catalyst surface. Thus H_2 production is improved by preventing photocorrosion and recombination of electrons and holes at the semiconductor surface. The superior photocatalytic activity was noted in the presence of glucose and went up to 103 μmol with an irradiation for 10 h whereas the value was just 16 μmol in the absence of glucose.

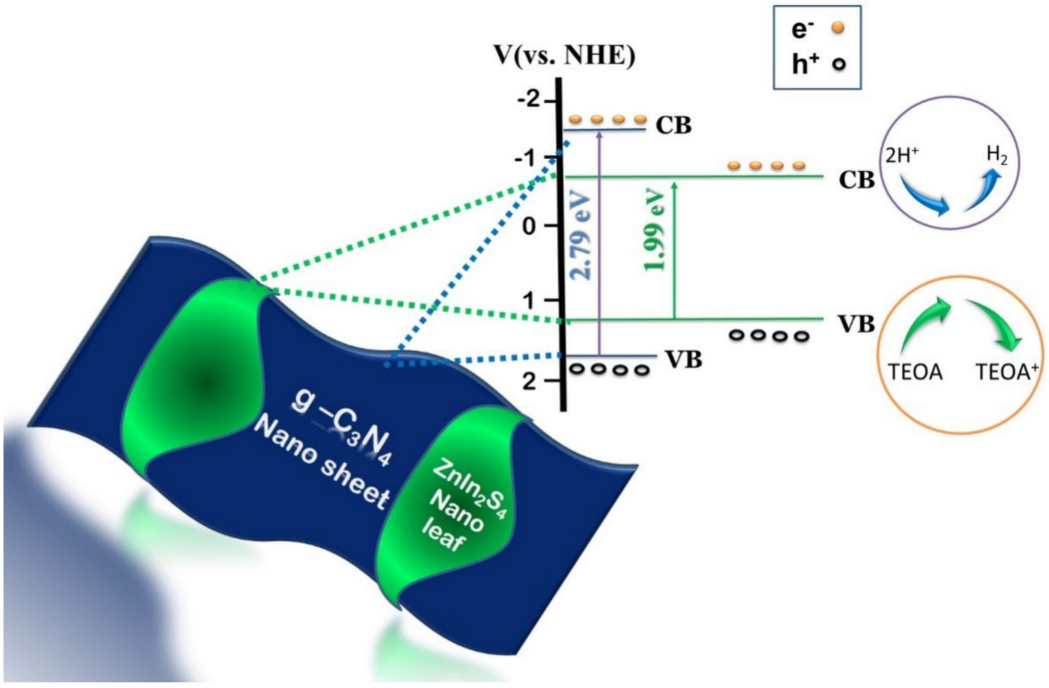

Figure 3. Schematic representation of in-situ growth of $ZnIn_2S_4$ nano leaves over g-C_3N_4 nanosheet. Figure adapted from [37].

5.2. Doping as a Strategy to Enhance Photocatalysis

Doping is generally considered a common strategy in boosting up the spectral response of a semiconductor. Commonly, doping an element into a semiconductor could narrow the bandgap and enhance the light-absorption ability [63,68]. Owing to the special electronic configuration of rare earth elements (REEs) with vacant f orbital, doping of rare-earth ions

has attracted research interest in the field of photocatalysis. Fien et al., (2014), has doped a series of RE ions (La^{3+}, Ce^{3+}, Er^{3+}, Gd^{3+}, Y^{3+}) into the lattice of $ZnIn_2S_4$ [38]. In their study, the photocatalytic H_2 production efficiency was observed to increase in the order of La-$ZnIn_2S_4$>Ce-$ZnIn_2S_4$>Er-$ZnIn_2S_4$>Gd-$ZnIn_2S_4$>Y-$ZnIn_2S_4$ post modification of $ZnIn_2S_4$ with RE ions. The decreasing number of electrons in the rare-earth 4f shell was consistent with the increased photocatalytic activity. REEs existed as RE_2O_3 oxide and modified the lattice of $ZnIn_2S_4$, increased its surface area and introduced defects on the catalyst surface, thus inhibiting recombination of photogenerated charge carriers. $ZnIn_2S_4$ lattice was also modified with La^{3+} for H_2 evolution activity [39]. Compared to pure $ZnIn_2S_4$, the H_2 evolution could be increased by 141.6% for 1 wt% La-doped samples. Zhu et al., (2017) on the other hand introduced reduced graphene oxide (RGO) and La into $ZnIn_2S_4$ lattice [43] and used Pt as co-catalyst for H_2 evolution. Among a series of samples synthesized by them, 1.0 Pt/1.0RGO/1.0 La-$ZnIn_2S_4$ gave the highest productivity of 2255 μmol g^{-1} h^{-1}. It was claimed that RGO could transfer the photoexcited electrons which are easily captured by the surface defects produced by La modification on $ZnIn_2S_4$ to generate H_2. Shen et al., (2012) modified $ZnIn_2S_4$ with series of alkaline earth (AE) metals (Ca, Ba, Sr) [49]. Among the AE-modified samples, only Ca incorporated samples show higher photocatalytic activity than pure $ZnIn_2S_4$, while the other two samples perform similar to bare samples. The variation in the photocatalytic performance was analyzed on the basis of UV-Vis spectroscopy and photoluminesce spectra. From UV-Vis absorption spectra it was clear that all samples exhibited the same profile with an intense absorption edge at 500 nm post-incorporation of AE. However, photoluminescence (PL) show decreased emission intensities in the order of $ZnIn_2S_4$>Ca– $ZnIn_2S_4$>Sr– $ZnIn_2S_4$>Ba– $ZnIn_2S_4$. It is expected that the introduction of AE ions could produce surface defects acting as trap centers for electrons, improving the charge separation and leading to a higher photocatalytic performance by Ba– $ZnIn_2S_4$ sample. However, only Ca- $ZnIn_2S_4$ exhibits better performance. This contradiction is explained by the defect emission peaks in the PL spectra at about 400–450 nm. Quenching in the native defect peaks relates to more non-radiative recombination in the system. Hence, both Ba and Sr doped samples possess fewer electrons and holes involved in photocatalysis thereby showing decreased efficiency in H_2 evolution [49]. An enhancement in photocatalytic activity post-incorporation of different transition metal (Cr, Mn, Fe, Co) ions into the lattice of $ZnIn_2S_4$ [54] is also investigated. The effect of Mn, Cr, Fe and Co doping on photocatalytic activity is analyzed on the basis of band structure and photoluminescence properties. The enhanced performance of the Mn-doped sample is attributed to the increased number of electrons and holes for photocatalysis induced by Mn doping. However, the decreased photocatalytic activity for Fe, Cr, Co-doped samples is attributed to the impurity levels created in the band-gap region which act as non-radiative recombination centers for photogenerated electrons and holes. Shen et al., (2008) analyzed the photocatalytic activity of Cu-doped $ZnIn_2S_4$ for H_2 evolution application [55]. Incorporating Cu in $ZnIn_2S_4$ lattice increased hydrogen evolution up to 151.5 μmol h^{-1} under visible light irradiation. Similar behavior could be observed upon Ni incorporation (Jing et al., (2010)) Ni^{2+} existed in NiS state post doping with its energy level lying close to the valence band of S3p orbital (see Figure 4) and acts as trapping sites for photogenerated holes while getting oxidized to Ni^{3+} state. Due to the instability of Ni^{3+}, it reverts back to Ni^{2+} state by releasing a hole. Thus, the shallow trapping of holes can extend the lifetime of the charge carrier separation and promote enhancement in the photocatalytic activity [56].

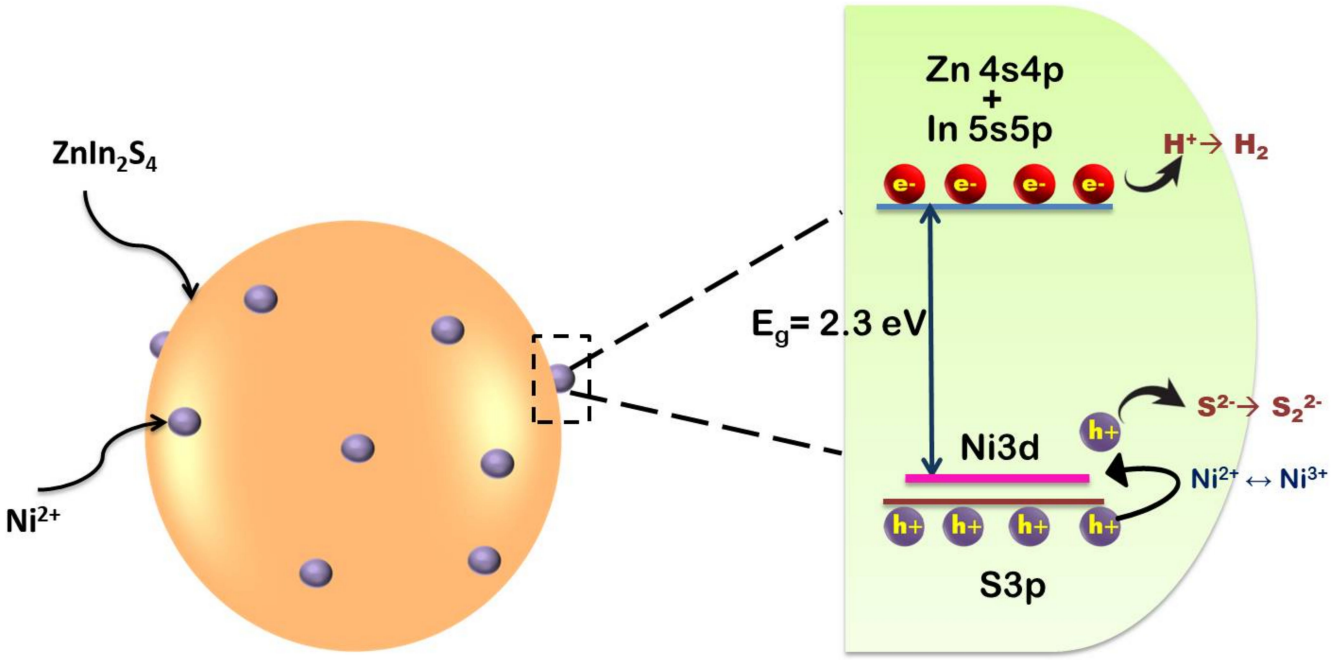

Figure 4. Schematic for band structure of Ni^{2+} doped $ZnIn_2S_4$. Figure adapted from [56].

5.3. Morphology and Porosity

Shape, size and structure of a material have a strong correlation with its physical and chemical properties. Thus tuning the shape and size of semiconductor photocatalyst could be a practical approach in controlling their photocatalytic activity. A simple solution chemistry route has been proposed by Gou et al., (2005) for the shape-controlled synthesis of $ZnIn_2S_4$ of various dimensions [31]. With the combination of hydrothermal, solvothermal and surfactant template techniques well-defined morphology of $ZnIn_2S_4$ could be achieved. This includes the synthesis of materials with various morphologies such as nanotubes, nanowires, nanoribbons, microspheres etc. For the nanoribbons, the solvothermal route has been used with pyridine as the solvent with a synthesis temperature >180 °C, while for the nanotubes, the synthesis temperature was lowered to <160 °C. Microspheres of $ZnIn_2S_4$ composed of irregular sheets were obtained when the solvent is replaced with water. The as-synthesized nano and microstructures exhibit modified optical properties with strong absorption from the UV to the visible range. Chaudhari et al., (2011) has proposed a detailed mechanism to control the microsphere shaped morphology of $ZnIn_2S_4$ by varying the solvent concentration (see Figure 5) [32]. In their study, (TEA), the sample exhibited marigold like morphology with curved petals in absence of triethylamine (TEA), while the sample with 0.005 mol of TEA possessed marigold morphology with increased puffiness. On further increasing the concentration of TEA to 0.01 mol, the entire flower-like morphology was drastically suppressed to smaller plates. It is proposed that the excess TEA could increase the bonding strength between TEA and surface atoms of $ZnIn_2S_4$ easily breaking down the Van der Waals force exerted between the petals. This accounts for the formation of nanoplates instead of micron-sized flowers. With TEA ~0.015 mol accelerated growth of unidimensional structures, like nanostrips, could also be achieved. Among $ZnIn_2S_4$ samples synthesized with various morphologies, H_2 evolution was higher (about 5287 μmol h^{-1}) in the case of the sample prepared with 0.01 mol of TEA with flower-like morphology.

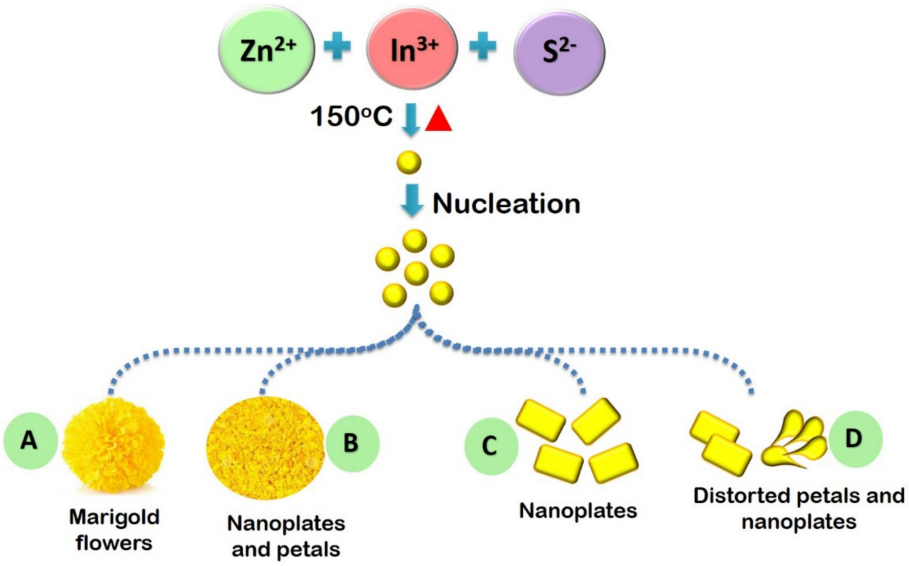

Figure 5. Schematic illustration of the growth of $ZnIn_2S_4$ with different solvent concentrations. Figure adapted from [32].

Lin et al., (2018) designed a heterojunction between 2D g-C_3N_4 nanosheets and 2D $ZnIn_2S_4$ nano leaves via facile surfactant-assisted solvothermal method for enhanced photo-induced H_2 generation [37]. From the as-synthesized bulk g-C_3N_4, thinner g-C_3N_4 nanosheets are exfoliated through the thermal oxidation process. These exfoliated nanosheets can help in constraining the vertical movement of charge carriers and facilitate recombination resistance [36]. $ZnIn_2S_4$ nano leaves were extracted from bulk $ZnIn_2S_4$ microspheres with the help of trisodium citrate dihydrate. These structures mimicking leaves from nature are expected to be beneficial for charge separation and promotion of improved photocatalytic H_2 generation. A combination of these two 2D structures, could create effective heterojunction with high-speed charge transportation and migration with enhanced photocatalytic activity. The effort of Tian et al., (2014) in modifying $ZnIn_2S_4$ with REEs had significant influence on the morphology and porous nature of the material. Unmodified $ZnIn_2S_4$ possessed gully-ball like spherical structures with collapsed nanosheets. When Y^{3+} was added, the surface of $ZnIn_2S_4$ was partially open with pores ranging between 0.3 µm to 0.5 µm. The addition of Gd^{3+} could open up the surface with many porous sheets to a given rose-like structure, while the addition of Er^{3+} and Ce^{3+} opened up the entire surface with a reduced gap possessing porous nanosheets ranging from 0.1 µm to 0.2 µm. A regular morphology with a fully opened sphere was observed with the addition of La^{3+}. This shows that the addition of rare earth ions onto the surface of $ZnIn_2S_4$ significantly modifies the surface with more regular, stabilized textures arresting agglomeration and maintaining mesopores. Their findings can be related to the fact that the addition of REEs promote-opening of porous structures with a decreased gap between nanosheets, increased surface area and pore volume providing better photocatalytic activity than pure $ZnIn_2S_4$ [38]. Solvent mediated synthesis of $ZnIn_2S_4$ by Shen et al., (2008) provides new insights on the effect of solvents on the morphology, crystallinity and photocatalytic properties of $ZnIn_2S_4$ [50]. Samples synthesized with H_2O as solvent presented a flowering-cherry-sphere-like structure with numerous petals. MeOH mediated synthesis resulted in smaller compact spheres with reduced petal length and thickness. Under ethylene glycol mediated condition, the sample did not show flower-like structure but presented clusters of irregular sheets. These results suggested that different organic solvents would hinder the growth of $ZnIn_2S_4$ and affect crystallinity. It was observed that the aqueous mediated sample showed regular morphology with good crystallinity and the highest photocatalytic activity among all the samples.

5.4. Role of Sacrificial Agent

Sacrificial agents play a prominent role in photocatalytic H_2 production reaction. Many reports suggest that the efficiency of a photocatalyst also relies on the nature of the sacrificial agent. In case of sulfide photocatalyst, amines and sulfide/sulfite-based sacrificial agents can get easily adsorbed on the surface of the catalyst and consume holes when compared to alcohols and sugar. The use of alcohols and sugars produces a neutral pH medium while amines and mixtures of sulfide and sulfite produce a high alkaline medium which is preferential for efficient H_2 production [71,72]. Li et al., (2010) in their work have used biomass glucose as an electron donor. From the viewpoint of renewable sources, they claim that glucose from cellulose or starch, when used as an electron donor, is far better when compared to S^{2-} obtained from sulfide/sulfite mixtures. Here, the H_2 production experiment with $ZnS/ZnIn_2S_4$ has been conducted with and without the usage of glucose as an electron donor. In the absence of glucose, it is noted that the H_2 production is saturated after a certain time whereas, a substantial increase in the rate of H_2 production is noted in the presence of glucose. In absence of glucose, S^{2-} generated from ZnS photocatalyst acts as a sacrificial agent for H_2 generation. In the presence of glucose, a proportional increase of H_2 with respect to light irradiation was observed. This is attributed to the fact that glucose acts as a direct hole scavenger inhibiting photo corrosion leading to an enhancement in photoactivity [28]. Similarly, several other hole scavengers such as KOH, triethylamine, lactic acid have also been used for H_2 production with sulfide-based photocatalysts [32,35,37,42].

6. Compounds with AB_2X_4 Structure Other than $ZnIn_2S_4$

Several multi-metal sulfide photocatalysts have been reported for water splitting applications using various sacrificial agents (see Figure 6). It is mainly attributed to the electronic properties of sulfide materials having conduction band composed of d, s, p orbitals and valence band having S3p orbitals which are negative compared to 2p orbitals of oxide materials. Hence sulfide materials possess band positions negative enough than oxides to reduce water to hydrogen. In addition, their narrow bandgap helps to cover the maximum of the solar spectrum [73]. Table 2 summarizes various such sulfide photocatalysts with AB_2X_4 structure (besides $ZnIn_2S_4$).

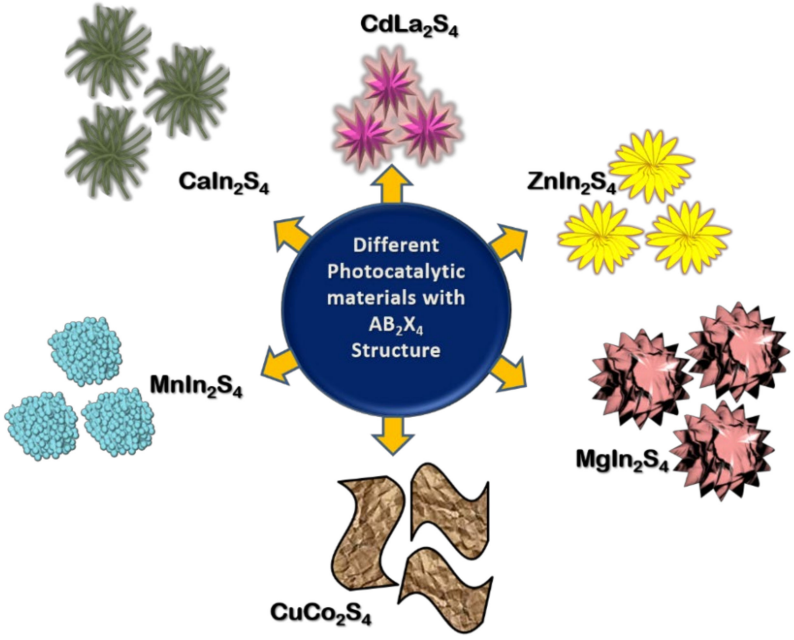

Figure 6. Representation of the morphologies of photocatalytic materials with AB_2X_4 structure.

Table 2. Other ternary metal sulfides and composites for photocatalytic H_2 generation with respective parameters.

S. No.	Photocatalys	Synthesis Method	Morphology	Co-Catalyst Used	Light Source	Sacrificial Agent	Catalyst Mass Used (g)	Yield (μmol h^{-1})	Ref.
1.	$CaIn_2S_4$	Hydrothermal	Irregular grains	-	300 W Xe lamp	-	0.05	30.92 (μmol g^{-1} h^{-1})	[74]
2.	$CdLa_2S_4$	Hydrothermal	Nanoprism and nanowires	-	450 W Xe lamp	Methanol	00.01	2252	[75]
3.	$MnIn_2S_4/gC_3N_4$	Hydrothermal	Nanoflakes	-	300 W Xe lamp	Na_2SO_3/Na_2S	0.03	200.8 (μmol g^{-1} h^{-1})	[76]
4.	$MnIn_2Se_4$	Hydrothermal	Nanosheets	$CoSeO_3$	300 W Xe lamp	Na_2SO_3/Na_2S	-	319 (μmol g^{-1} h^{-1})	[77]
5.	$MgIn_2S_4$/ polyaniline	Solvothermal	Flower like microsphere with nanosheets	-	300 W Xe lamp	-	-	17.53 (μmol g^{-1} h^{-1})	[78]
6.	$g\text{-}C_3N_4/CaIn_2S_4$	Hydrothermal	Thin and irregular nanosheets with wrinkles	-	300 W Xe lamp	Na_2SO_3/Na_2S	0.05	102	[79]
7.	1wt%CdS-$CdLa_2S_4$	Solvothermal	Submicrosphere consisting of nanoprism	-	300 W Xe lamp	Na_2SO_3/Na_2S	0.2	500	[80]
8.	3wt%CdS-$CdLa_2S_4$	Solvothermal	Submicrosphere consisting of nanoprism	-	300 W Xe lam	Na_2SO_3/Na_2S	0.2	2280	[80]
9.	5wt%CdS-$CdLa_2S_4$	Solvothermal	Submicrosphere consisting of nanoprism	-	300 W Xe lam	Na_2SO_3/Na_2S	0.2	1420	[80]
10.	$CdIn_2S_4$	Hydrothermal	Microsphere with nanopetals and nanotubes	-	450 W Xe lamp	KOH (photodecomposition of H_2S)	0.5	6960 (μmol g^{-1} h^{-1})	[81]
11.	$CdIn_2S_4$	Surfactant assisted hydrothermal	Microsphere with nanopetals	-	300 W Xe lamp	KOH (photodecomposition of H_2S)	0.5	6476 (μmol g^{-1} h^{-1})	[81]
12.	$CuCo_2S_4$	Hydrothermal	2D nanosheet like morphology	-	250 W Mercury lamp	Na_2SO_3/Na_2S	0.06	25900 (μmol g^{-1} h^{-1})	[70]

To enhance the performance of sulphide photocataysts, several techniques such as, doping, creating heterojunctions, introducing sacrificial agents and co-catalysts have been followed. $CaIn_2S_4$ has been proposed as an efficient photocatalyst for H_2 generation by Ding et al., (2013) and a modification of $CaIn_2S_4$ with g-C_3N_4 has been proposed by Jiang et al., (2015) [74,79]. Jiang et al., (2015) elucidates the enhanced photocatalytic performance of $CaIn_2S_4$/g-C_3N_4 heterostructure through H_2 production and degradation of textile dye methyl orange. Two-dimensional g-C_3N_4/cubic $CaIn_2S_4$ based heterojunctions provide interfacial contact which promotes charge separation to facilitate enhanced photoactivity. Pt co-catalyst assisted H_2 production with 30% $CaIn_2S_4$/g-C_3N_4 nanocomposite resulted in H_2 evolution rate of 102 μmol g^{-1} h^{-1} (three times higher than that of pristine $CaIn_2S_4$) [79]. Kale et al., (2006) synthesized $CdIn_2S_4$ with fine marigold-like morphology through aqueous-mediated hydrothermal method and two-dimensional nanotubes morphology with the diameter of 25 nm, through methanol-mediated solvothermal process. In the H_2 evolution reaction, a quantum yield of 16.8% was achieved in the case of marigold-like morphology while 17.1% was achieved for $CdIn_2S_4$ with nanotube morphology [81]. NiS_2 nanoparticles were deposited onto $CdLa_2S_4$ nanocrystals as co-catalyst for the enhancement of photocatalytic activity. The NiS_2 loaded sample resulted in significant enhancement for H_2 production under visible light irradiation. Compared to the pristine $CdLa_2S_4$, 2 wt% NiS_2 loading sample exhibited three times higher H_2 production rate up to 2.5 mmol g^{-1} h^{-1} [82]. Interesting morphologies like self-assembled nanohexagon flowers, nanoprisms and nanowires for $CdLa_2S_4$ were demonstrated through facile hydrothermal synthesis by varying the reaction medium with water and methanol. A wide variation in morphologies attained from highly crystalline 3D nanoprisms to 1D nanowires showed the influence of the reaction medium during synthesis (Figure 7). The optical band gap of bare nanoprisms, nanowires, nanohexagon flowers and nanoplates of $CdLa_2S_4$ range from 2.1 eV to 2.3 eV and are active under the visible region of the solar spectrum. $CdLa_2S_4$ with 3D prism morphology generated maximum amount of H_2 up to 2552 mmol $h^{-1}g^{-1}$ [75].

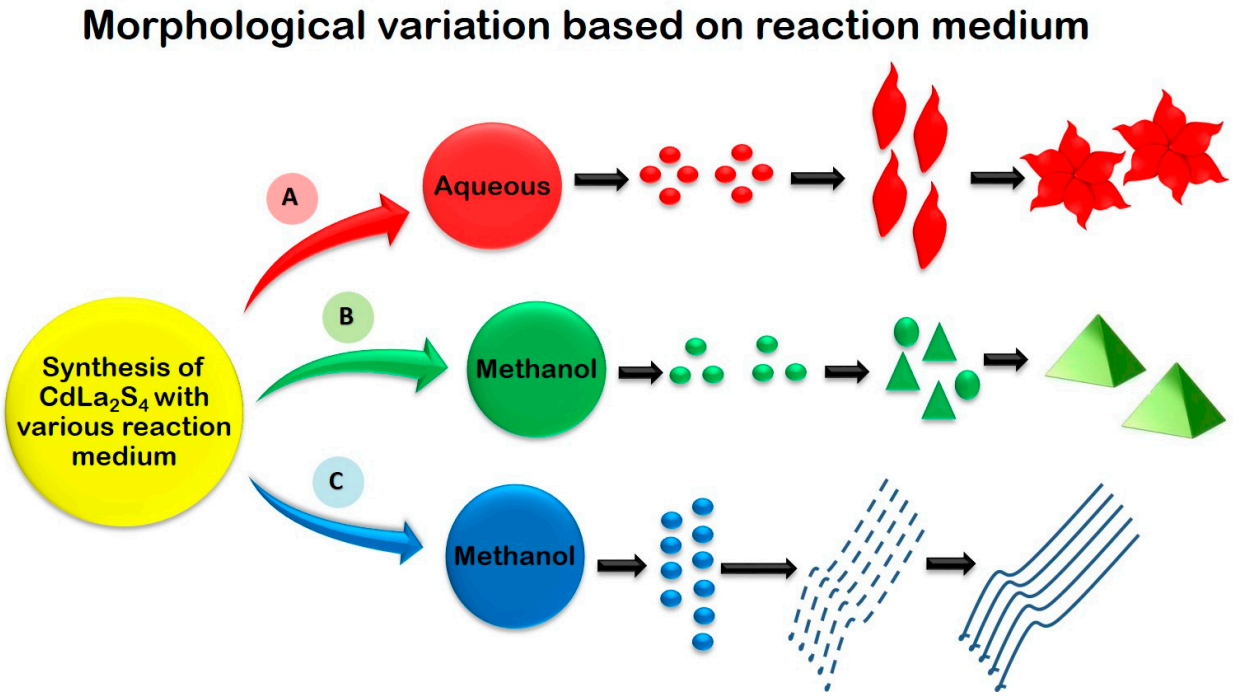

Figure 7. Schematic representation of various morphologies of $CdLn_2S_4$ obtained by controlling the reaction medium and their corresponding concentration. Figure adapted from [74].

CdS nanocrystals incorporated $CdLa_2S_4$ microspheres with 0.4 wt% of Pt as co-catalyst showed a high H_2-production rate of 2.25 mmol h^{-1} [80]. Magnesium-based chalcogenide

photocatalyst $MgIn_2S_4$, on the other hand, when integrated with polyaniline (PANI) proves to be an efficient H_2 generating photocatalyst [78]. PANI/$MgIn_2S_4$ nanoflower photocatalysts with 1% PANI loading synthesized through facile chemisorption method exhibits a decent H_2 evolution of 200.8 μmol g^{-1} h^{-1} under visible light irradiation. Chauhan et al., (2019) reported co-catalyst free $CuCo_2S_4$ nanosheets as a promising semiconductor photocatalyst for water splitting reactions under visible light irradiation. A simple hydrothermal route was adapted for the synthesis of nanosheets, exhibiting an appropriate band-gap of 2.24 eV. A quantum yield of 2.48% was achieved for the photo-catalytically active $CuCo_2S_4$ nanosheets under visible light and it exhibited excellent weight-normalized photoactivity generating H_2 at the rate of ~25,900 μmol g^{-1} h^{-1}. $CuCo_2S_4$ nanosheets have been considered important due to the extraordinary long-term operational stability up to 12 h study time without using any co-catalyst [70,71].

7. Conclusions

It is observed from the review that, tremendous efforts have been put up in exploring sulfide photocatalysts and improving their efficiency in the past several decades. It is necessary for an ideal photocatalyst to have higher efficiency with excellent solar spectrum response to be applicable at the industrial level. REEs semiconductors are known for their narrow band gaps and superior photoresponse. Moreover, many promising strategies for enhancing the performance of the catalyst by introducing foreign elements, integrating suitable semiconductors to form heterojunctions, etc are being explored. At this stage, it is necessary to address the key issue of enhancing the H_2 production efficiency of sulfur-based photocatalysts. Intensive investigations need to be carried out in improving the behavior of photogenerated electrons and holes which could be affected by crystallinity, surface states, defects and morphology of the semiconductor. The lack of extensive experiments for scaling-up the efficiency of sulfides to promote laboratory research to industrial-scale needs to be overcome through systematic research. Among various sulfide catalysts, $ZnIn_2S_4$ is an emerging ternary metal chalcogenide photocatalyst with excellent features such as good crystallinity, porous hierarchical morphology, optical properties, easy fabrication and eco-friendly nature. Despite encouraging properties, $ZnIn_2S_4$ based compounds as a photocatalyst face many challenges. However, with its certain superior and moldable properties can be considered as a promising material for photo-assisted applications in the future.

Author Contributions: Conceptualization, R.J.; data collection, R.J. and R.P.V.; Manuscript preparation, R.J., R.P.V., A.R., S.S. and C.-T.C.; Revision, R.J., R.P.V., A.R., S.S. and C.-T.C.; Figure contribution, R.P.V. and A.R.; Schematic design, A.R.; Review, S.S. and C.-T.C.; Funding acquisition, S.S. and C.-T.C. Corresponding author-responsible for ensuring that the descriptions are accurate and agreed by all authors. All authors have read and agreed to the published version of the manuscript.

Funding: This work was financially supported by grant funded from MOST-108-2622-E-197-003-CC3 Taiwan.

Acknowledgments: Shubra Singh would like to acknowledge University Grants Commission (UGC), DST Solar Energy Harnessing Center-DST/TMD/SERI/HUB/1(C) and DST/TMD-EWO/WTI/2K19/EWFH/2019/122. R. Janani would like to acknowledge the SERB project [EMR/2017/000794].

Conflicts of Interest: The author declare no conflict of interest.

References

1. Fujishima, A.; Honda, K. Electrochemical photolysis of water at a semiconductor electrode. *Nature* **1972**, *238*, 37–38. [CrossRef]
2. Ismael, M. A review and recent advances in solar-to-hydrogen energy conversion based on photocatalytic water splitting over doped-TiO_2 nanoparticles. *Sol Energy* **2020**, *211*, 522–546. [CrossRef]
3. Acar, C.; Dincer, I.; Naterer, G.F. Review of photocatalytic water-splitting methods for sustainable hydrogen production. *Int. J. Energy Res.* **2016**, *40*, 1449–1473. [CrossRef]
4. Fajrina, N.; Tahir, M. A critical review in strategies to improve photocatalytic water splitting towards hydrogen production. *Int. J. Hydrog. Energy* **2019**, *44*, 540–577. [CrossRef]

5. Lui, J.; Chen, W.H.; Tsang, D.C.W.; You, S. A critical review on the principles applications, and challenges of waste to hydrogen technologies. *Renew. Sustain. Energy Rev.* **2020**, *134*, 110365. [CrossRef]
6. Singla, S.; Sharma, S.; Basu, S.; Nagaraj, P.; Kakarla, S.; Reddy, R. graphene/graphitic carbon notride- based ternary nanohybrids: Synthesis methods, properties, and applications for photocatlytic hydrogen production. *FlatChem* **2020**, *24*, 100200. [CrossRef]
7. Gupta, N.M. Factors affecting the efficiency of a water splitting photocatalyst: A perspective. *Renew. Sustain. Energy Rev.* **2017**, *71*, 585–601. [CrossRef]
8. Liang, Z.; Shen, R.; Ng, H.Y.; Zhang, P.; Xiang, Q.; Li, X. A review on 2D MoS_2 cocatalysts in photocatalytic H_2 production. *J. Mater. Sci. Technol.* **2020**, *56*, 89–121. [CrossRef]
9. Tasleem, S.; Tahir, M. Current trends in strategies to improve photocatalytic performance of perovskites materials for solar to hydrogen production. *Renew. Sustain. Energy Rev.* **2020**, *132*, 110073. [CrossRef]
10. Morillo, E.S.; Toledo, N.M.; Luisa, J.; Fierro, G.; Rufino, M.; Yerga, N. Role of the Sulphur Source in the Solvothermal Synthesis of Ag-CdS Photocatalysts: Effects on the Structure and Photoactivity for Hydrogen Production. *Hydrogen* **2020**, *1*, 64–89. [CrossRef]
11. Saleem, Z.; Pervaiz, E.; Yousaf, M.U.; Niazi, M. Two-Dimensional Materials and Composites as Potential Water Splitting Photocatalysts: A Review. *Catalysts* **2020**, *10*, 464. [CrossRef]
12. Martín, S.S.; Rivero, M.J.; Ortiz, I. Unravelling the Mechanisms that Drive the Performance of Photocatalytic Hydrogen Production. *Catalysts* **2020**, *10*, 901. [CrossRef]
13. Wang, S.; Ding, Z.; Chang, X.; Xu, J.; Wang, D.H. Modified Nano-TiO_2 Based Composites for Environmental Photocatalytic Applications. *Catalysts* **2020**, *10*, 759. [CrossRef]
14. Lee, S.L.; Chang, C.J. Recent Progress on Metal Sulfide Composite Nanomaterials for Photo Catalytic Hydrogen Production. *Catalysts* **2019**, *9*, 457. [CrossRef]
15. Li, J.; Calvo, P.J.; Paineau, E.; Ghazzal, M.N. Metal Chalcogenides Based Heterojunctions and Novel Nanostructures for Photocatalytic Hydrogen Evolution. *Catalysts* **2020**, *10*, 89. [CrossRef]
16. Jafari, T.; Moharreri, E.; Amin, A.Z.; Miao, R.; Song, W.; Suib, S.L. Photocatalytic Water Splitting—The Untamed Dream: A Review of Recent Advances. *Molecules* **2016**, *21*, 900. [CrossRef]
17. Sato, J.; Saito, S.; Nishiyama, H.; Inoue, Y. New Photocatalyst Group for Water Decomposition of RuO_2-Loaded p-Block Metal (In, Sn, and Sb) Oxides with d10 Configuration. *J. Phys. Chem. B* **2001**, *105*, 6061. [CrossRef]
18. Ikarashi, K.; Sato, J.; Kobayashi, H.; Saito, S.; Nishiyama, H.; Inoue, Y. Photocatalysis for Water Decomposition by RuO_2-Dispersed $ZnGa_2O_4$ with d10 Configuration. *J. Phys. Chem. B* **2002**, *106*, 9048. [CrossRef]
19. Sato, J.; Saito, S.; Nishiyama, H.; Inoue, Y. Photocatalytic Activity for Water Decomposition of Indates with Octahedrally Coordinated d10 Configuration. I. Influences of Preparation Conditions on Activity. *J. Phys. Chem. B* **2003**, *107*, 7965. [CrossRef]
20. Sato, J.; Kobayashi, H.; Inoue, Y. Photocatalytic Activity for Water Decomposition of Indates with Octahedrally Coordinated d10 Configuration. II. Roles of Geometric and Electronic Structures. *J. Phys. Chem. B* **2003**, *107*, 7970. [CrossRef]
21. Sato, J.; Kobayashi, H.; Ikarashi, K.; Saito, S.; Nishiyama, H.; Inoue, Y. Photocatalytic Activity for Water Decomposition of RuO2-Dispersed Zn2GeO4 with d10 Configuration. *J. Phys. Chem. B* **2004**, *108*, 4369. [CrossRef]
22. Kadowaki, H.; Saito, N.; Nishiyama, H.; Inoue, Y. RuO_2-loaded Sr^{2+}-doped CeO_2 with d0 Electronic Configuration as a New Photocatalyst for Overall Water Splitting. *Chem. Lett.* **2007**, *36*, 440–441. [CrossRef]
23. Inoue, Y. Photocatalytic water splitting by RuO_2-loaded metal oxides and nitrides with d0- and d10 -related electronic configurations Energy Environ. *Science* **2009**, *2*, 364–386.
24. Chen, Z.; Xing, P.; Chen, P.; Chen, Q.; Wang, Y.; Yu, J.; He, Y. Synthesis of carbon doped $KTaO_3$ and its enhanced performance in photocatalytic H_2 generation. *Catal. Commun.* **2018**, *109*, 6–9. [CrossRef]
25. Iwashina, K.; Kudo, A. Rh-Doped $SrTiO_3$ Photocatalyst Electrode Showing Cathodic Photocurrent for Water Splitting under Visible-Light Irradiation. *J. Am. Chem. Soc.* **2011**, *133*, 13272–13275. [CrossRef]
26. Ahmad, H.; Kamarudin, S.K.; Minggu, L.J.; Kassim, M. Hydrogen from photo-catalytic water splitting process: A Review. *Renew. Sustain. Energy Rev.* **2015**, *43*, 599–610. [CrossRef]
27. Pareek, A.; Gopalakrishnan, A.; Borse, P.H. Efficiency and stability aspects of CdS photoanode for solar hydrogen generation technology. *J. Phys. Conf. Ser.* **2016**, *755*, 012006. [CrossRef]
28. Li, Y.; Wang, J.; Peng, S.; Lu, G.; Li, S. Photocatalytic hydrogen generation in the presence of glucose over ZnS-coated $ZnIn_2S_4$ under visible light irradiation. *Int. J. Hydrogen Energy* **2010**, *35*, 7116–7126. [CrossRef]
29. Seo, W.S.; Otsuka, R.; Okuno, H.; Ohta, M.; Koumoto, K. Thermoelectric properties of sintered polycrystalline $ZnIn_2S_4$. *J. Mater. Res.* **1999**, *14*, 4176–4181. [CrossRef]
30. Chen, Z.; Li, D.; Zhang, W.; Chen, C.; Li, W.; Sun, M.; He, Y.; Fu, X. Low-Temperature and Template-Free Synthesis of $ZnIn_2S_4$Microspheres. *Inorg. Chem.* **2008**, *47*, 9766–9772. [CrossRef]
31. Gou, X.; Cheng, F.; Shi, Y.; Zhang, L.; Peng, S.; Chen, A.J.; Shen, P. Shape-Controlled Synthesis of Ternary Chalcogenide $ZnIn_2S_4$ and $CuIn(S,Se)_2$ Nano-/Microstructures via Facile Solution Route. *J. Am. Chem. Soc.* **2006**, *128*, 7222–7229. [CrossRef]
32. Chaudhari, N.S.; Bhirud, A.P.; Sonawane, R.S.; Nikam, L.K.; Warule, S.S.; Rane, V.H.; Kale, B.B. Ecofriendly hydrogen production from abundant hydrogen sulfide using solar light-driven hierarchical nanostructured $ZnIn_2S_4$ photocatalyst. *Green Chem.* **2011**, *13*, 2500–2506. [CrossRef]
33. Romeo, N.; Dallaturca, A.; Braglia, R.; Sberveglieri, G. Charge storage in $ZnIn_2S_4$single crystals. *Appl. Phys. Lett.* **1973**, *22*, 21–22. [CrossRef]

34. Bai, X.; Li, J. Photocatalytic hydrogen generation over porous $ZnIn_2S_4$ microspheres synthesized via a CPBr-assisted hy-drothermal method. *Mater. Res. Bull.* **2011**, *46*, 1028–1034. [CrossRef]
35. Yang, M.-Q.; Xu, Y.-J.; Lu, W.; Zeng, K.; Zhu, H.; Xu, Q.-H.; Ho, G.W. Self-surface charge exfoliation and electrostatically coordinated 2D hetero-layered hybrids. *Nat. Commun.* **2017**, *8*, 14224. [CrossRef]
36. Zhenyi, Z.; Kuichao, L.; Zhiqing, F.; Yanan, B.; Bin, D. Hierarchical Sheet-on-Sheet $ZnIn_2S_4$/g-C_3N_4 Heterostructure with Highly Efficient Photocatalytic H_2 production Based on Photoinduced Interfacial Charge Transfer. *Sci Rep.* **2016**, *6*, 19221.
37. Lin, B.; Li, H.; An, H.; Hao, W.; Wei, J.J.; Dai, Y.; Ma, C.; Yang, G. Preparation of 2D/2D g-C_3N_4 nanosheet@ $ZnIn_2S_4$ nanoleaf heterojunctions with well-designed high-speed charge transfer nanochannels towards high-efficiency photocatalytic hydrogen evolution. *Appl. Catal. B* **2018**, *220*, 542–555. [CrossRef]
38. Tian, F.; Zhu, R.; He, Y.; Ouyang, F. Improving photocatalytic activity for hydrogen evolution over $ZnIn_2S_4$ under visi-ble-light: A case study of rare earth modification. *Int. J. Hydrog. Energy* **2014**, *39*, 6335–6344. [CrossRef]
39. Tian, F.; Zhu, R.; Song, K.; Ouyang, F.; Cao, G. The effects of amount of La on the photocatalytic performance of $ZnIn_2S_4$ for hydrogen generation under visible light. *Int. J. Hydrog. Energy* **2015**, *40*, 2141–2148. [CrossRef]
40. Pudkon, W.; Bahruji, H.; Miedziak, P.J.; Davies, T.E.; Morgan, D.J.; Pattisson, S.; Kaowphong, S.; Hutchings, G.J. Enhanced visible-light-driven photocatalytic H_2 production and Cr(vi) reduction of a $ZnIn_2S_4$/MoS_2 heterojunction synthesized by the biomolecule-assisted microwave heating method. *Catal. Sci. Technol.* **2020**, *10*, 2838–2854. [CrossRef]
41. Bai, X.; Danc, W.C.; Peng, W. Photodecomposition of H_2S to H_2 over $Cd_xZn_{1-x}S$ composite photocatalysts. *Rare Met.* **2009**, *28*, 2. [CrossRef]
42. Li, W.; Lin, W.; Yang, G. 2D self-assembled MoS_2/ $ZnIn_2S_4$ heterostructure for efficient photocatalytic hydrogen evolution. *Nanoscale* **2017**, *9*, 18290–18298. [CrossRef]
43. Zhu, R.; Tian, F.; Che, S.; Cao, G.; Ouyang, F. The photocatalytic performance of modified $ZnIn_2S_4$ with graphene and La for hydrogen generation under visible light. *Renew. Energy* **2017**, *113*, 1503–1514. [CrossRef]
44. Yuan, Y.J.; Tu, J.R.; Ye, Z.J.; Chen, D.Q.; Hub, B.; Huang, Y.W. MoS_2-graphene/ $ZnIn_2S_4$ hierarchical microarchitectures with an electron transport bridge between light-harvesting semiconductor and cocatalyst: A highly efficient photocatalyst for solar hydrogen generation. *Appl. Catal. B* **2016**, *188*, 13–22. [CrossRef]
45. Lei, Z.; You, W.; Liu, M.; Zhou, G.; Takata, T.; Hara, M.; Domen, K.; Li, C. Photocatalytic water reduction under visible light on a novel $ZnIn_2S_4$ catalyst synthesized by hydrothermal method. *Chem. Commun.* **2003**, 2142–2143. [CrossRef]
46. Chai, B.; Peng, T.; Zeng, P.; Zhang, X.; Liu, X. Template-Free Hydrothermal Synthesis of $ZnIn_2S_4$ Floriated Microsphere as an Efficient Photocatalyst for H2 Production under Visible-Light Irradiation. *J. Phys. Chem. C* **2011**, *115*, 6149–6155. [CrossRef]
47. Shen, S.; Zhao, L.; Guo, L. Cetyltrimethylammoniumbromide (CTAB) assisted hydrothermal synthesis of $ZnIn_2S_4$ as an efficient visible light drivenphotocatalyst for hydrogen production. *Int. J. Hydrog. Energy* **2008**, *33*, 4500–4510. [CrossRef]
48. Shen, S.; Zhao, L.; Guo, L. Crystallite, optical and photocatalytic properties of visible-light-driven $ZnIn_2S_4$ photocatalysts synthesized via a surfactant-assisted hydrothermal method. *Mater. Res. Bull.* **2009**, *44*, 100–105. [CrossRef]
49. Shen, S.; Zhao, L.; Guan, X.; Guo, L. Improving visible-light photocatalytic activity for hydrogen evolution over $ZnIn_2S_4$: A case study of alkaline-earth metal doping. *J. Phys. Chem. Solids* **2012**, *73*, 79–83. [CrossRef]
50. Shen, S.; Zhao, L.; Guo, L. Morphology, structure and photocatalytic performance of $ZnIn_2S_4$ synthesized via a sol-vothermal/hydrothermal route in different solvents. *J. Phys. Chem. Solids* **2008**, *69*, 2426–2432. [CrossRef]
51. Shen, S.; Guo, P.; Zhao, L.; Yuanchang, D.; Liejin, G. Insights into photoluminescence property and photocatalytic ac-tivity of cubic and rhombohedral $ZnIn_2S_4$. *J. Solid State Chem.* **2011**, *184*, 2250–2256. [CrossRef]
52. Chai, B.; Peng, T.; Zeng, P.; Zhang, X. Preparation of a MWCNTs/ $ZnIn_2S_4$ composite and its enhanced photocatalytic hydrogen production under visible-light irradiation. *Dalton Trans.* **2012**, *41*, 1179. [CrossRef]
53. Fan, W.J.; Zhou, Z.F.; Xu, W.B.; Shi, Z.F.; Ren, F.M.; Ma, H.H.; Huang, S.W. Preparation of $ZnIn_2S_4$/fluoropolymer fiber composites and its photocatalytic H_2 evolution from splitting of water using Xe lamp irradiation. *Int. J. Hydrog. Energy* **2010**, *35*, 6525–6530. [CrossRef]
54. Shen, S.; Chen, X.; Ren, F.; Kronawitter, C.X.; Mao, S.S.; Guo, L. Solar light-driven photocatalytic hydrogen evolution over $ZnIn_2S_4$ loaded with transition-metal sulfides. *Nanoscale Res. Lett.* **2011**, *6*, 1–6. [CrossRef]
55. Shen, S.; Zhao, L.; Zhou, Z.; Guo, L. Enhanced Photocatalytic Hydrogen Evolution over Cu-Doped $ZnIn_2S_4$ under Visible Light Irradiation. *J. Phys. Chem. C* **2008**, *112*, 16148–16155. [CrossRef]
56. Jing, D.; Liu, M.; Guo, L. Enhanced Hydrogen Production from Water over Ni Doped $ZnIn_2S_4$ Microsphere Photocatalysts. *Catal. Lett.* **2010**, *140*, 167–171. [CrossRef]
57. Chandrasekaran, S.; Yao, L.; Deng, L.; Bowen, C. Recent advances in metal sulfides: From controlled fabrication to elec-trocatalytic photocatalytic and photoelectrochemical water splitting and beyond. *Chem.Soc. Rev.* **2019**, *48*, 4178–4280. [CrossRef]
58. Rohrer, G.S. *Structure and Bonding in Crystalline Materials*; Amsterdam University Press: Amsterdam, The Netherlands, 2001.
59. Vaughan, D.J.; Corkhill, C.L. Mineralogy of Sulfides. *Elements* **2017**, *13*, 81–87. [CrossRef]
60. Hauck, J.; Mika, K. Ordering of Metal Atoms in Wurtzite and Sphalerite Structures. *J. Solid State Chem.* **1998**, *138*, 334–341. [CrossRef]
61. Pakiari, A.H.; Jamshidi, Z. Nature and Strength of M−S Bonds (M = Au, Ag, and Cu) in Binary Alloy Gold Clusters. *J. Phys. Chem. A* **2010**, *114*, 9212–9221. [CrossRef]

62. Yina, X.; Sheng, P.; Zhong, F.; Van Nguyen, M.; Cai, Q.; Grimes, C. CdS/$ZnIn_2S_4$/TiO_2 3D-Heterostructures and Their Photoelectrochemical Properties. *New J. Chem.* **2016**, *40*, 6675–6685. [CrossRef]
63. Pan, Y.; Yuan, X.; Jiang, L.; Yu, H.; Zhang, J.; Wang, H.; Guan, R.; Guangming, Z. Recent advances in synthesis, modi-fication and photocatalytic application of micro/nano-structured zinc indium sulfide. *Chem. Eng. J.* **2018**, *354*, 407–431.
64. Chen, J.; Xin, F.; Yin, X.; Xiang, T.; Wang, Y. Synthesis of hexagonal and cubic $ZnIn_2S_4$ nanosheets for the photocatalytic reduction of CO_2 with methanol. *RSC Adv.* **2015**, *5*, 3833. [CrossRef]
65. Mohamed, R.M.; Shawky, A.; Aljahdali, M.S. Palladium/zinc indium sulfide microspheres: Enhanced photo-catalysts prepare methanol under visible light conditions. *J. Taiwan Inst. Chem. Eng.* **2016**, *65*, 498–504. [CrossRef]
66. Chen, J.; Xin, F.; Niu, H.; Mao, C.J.; Song, J.M. Photocatalytic reduction of CO_2 with methanol over Bi_2S- $ZnIn_2S_4$ nano-composites. *Mat. Lett.* **2017**, *198*, 1–3. [CrossRef]
67. Zhang, Y.J.; Tang, H.M.; Gao, S.-P. Density Functional Theory Study of $ZnIn_2S_4$ and $CdIn_2S_4$ Polymorphs Using Full-Potential Linearized Augmented Plane Wave Method and Modified Becke—Johnson Potential. *Phys. Status Solidi B* **2020**, *257*, 1900485. [CrossRef]
68. Janani, R.; Priyanga, G.; Behara, S.; Melwin, A.A.; Shaheer, A.; Thomas, T.; Neppolian, B.; Singh, S. Enhanced solar light driven hydrogen generation and environment remediation through Nd incorporated $ZnIn_2S_4$. *Renew. Energy* **2020**, *162*, 2031–2040. [CrossRef]
69. Kudo, A.; Miseki, Y. Heterogeneous photocatalyst materials for water splitting. *Chem. Soc. Rev.* **2009**, *38*, 253–278. [CrossRef]
70. Chauhan, M.; Soni, K.; Karthik, P.E.; Reddy, K.P.; Gopinath, C.S.; Deka, S. Promising visible-light driven hydrogen production from water on a highly efficient $CuCo_2S_4$ nanosheet photocatalyst. *J. Mater. Chem. A* **2019**, *7*, 6985–6994. [CrossRef]
71. Li, L.; Xu, J.; Ma, J.; Liu, Z.; Li, Y. A bimetallic sulfide $CuCo_2S_4$ with good synergistic effect was constructed to drive high performance photocatalytic hydrogen evolution. *J. Colloid Interface Sci.* **2019**, *552*, 17–26. [CrossRef]
72. Kumaravel, V.; Imam, M.D.; Badreldin, A.; Chava, R.K.; Do, J.Y.; Kang, M.; Wahab, A.A. Photocatalytic hydrogen pro-duction: Role of sacrificial agents on the activity of oxide, carbon, and sulfide catalysts. *Catalysts* **2019**, *9*, 276. [CrossRef]
73. Zhang, K.; Guo, L. Metal sulfide semiconductor for photocatalytic hydrogen production. *Catal. Sci. Technol.* **2013**, *3*, 1672–1690. [CrossRef]
74. Ding, J.; Sun, S.; Yan, W.; Bao, J.; Gao, C. Photocatalytic H_2 evolution on a novel $CaIn_2S_4$ photocatalyst under visible light irradiation. *Int. J. Hydrog. Energy* **2013**, *30*, 13153–13158. [CrossRef]
75. Kale, B.B.; Baeg, J.-O.; Kong, K.-J.; Moon, S.-J.; Nikam, L.K.; Patil, K.R. Self assembled $CdLa_2S_4$ hexagon flowers, nanoprisms and nanowires: Novel photocatalysts for solar hydrogen production. *J. Mater. Chem.* **2011**, *21*, 2624–2631. [CrossRef]
76. Chen, W.; He, Z.-C.; Huang, G.-B.; Wu, C.-L.; Chen, W.-F.; Liu, X.-H. Direct Z-scheme 2D/2D $MnIn_2S_4$/g-C_3N_4 architectures with highly efficient photocatalytic activities towards treatment of pharmaceutical wastewater and hydrogen evolution. *Chem. Eng. J.* **2019**, *359*, 244–253. [CrossRef]
77. Liang, H.; Feng, T.; Tan, S.; Zhao, K.; Wang, W.; Dong, B.; Cao, L. Two-dimensional (2D) $MnIn_2Se_4$ nanosheets with porous structure: A novel photocatalyst for water splitting without sacrificial agents. *Chem. Commun.* **2019**, *55*, 15061–15064. [CrossRef] [PubMed]
78. Jing, L.; Xu, Y.; Xie, M.; Liu, J.; Deng, J.; Huang, L.; Xu, H.; Li, H. Three dimensional polyaniline/$MgIn_2S_4$ nanoflower photocatalysts accelerated interfacial charge transfer for the photoreduction of Cr(VI), photodegradation of organic pollution and photocatalytic H_2 production. *Chem. Eng. J.* **2019**, *360*, 1601–1612. [CrossRef]
79. Jiang, D.; Li, J.; Xing, C.; Zhang, Z.; Meng, S.; Chen, M. Two-Dimensional $CaIn_2S_4$/g-C_3N_4 Heterojunction Nanocomposite with Enhanced Visible-Light Photocatalytic Activities: Interfacial Engineering and Mechanism Insight. *ACS Appl. Mater. Interfaces* **2015**, *34*, 19234–19242. [CrossRef] [PubMed]
80. Hou, J.; Yang, C.; Wang, Z.; Jiao, S.; Zhu, H. Hydrothermal synthesis of CdS/$CdLa_2S_4$ heterostructures for efficient visi-ble-light driven photocatalytic hydrogen production. *RSC Adv.* **2012**, *2*, 10330–10336. [CrossRef]
81. Kale, B.B.; Baeg, J.O.; Lee, S.M.; Chang, H.; Moon, S.J.; Lee, C.W. $CdIn_2S_4$ Nanotubes and "Marigold" Nanostruc-tures: A Visible-Light Photocatalyst. *Adv. Funct. Mater.* **2006**, *16*, 1349–1354. [CrossRef]
82. Yuan, P.Y.; Cao, W.S.; Yin, S.L.; Xu, L.; Xue, C. NiS_2 Co-catalyst decoration on $CdLa_2S_4$ nanocrystals for efficient photo-catalytic hydrogen generation under visible light irradiation. *Int. J. Hydrog. Energ.* **2013**, *38*, 7218–7223. [CrossRef]